Influence of laser pulse width to the photoacoustic temporal waveform and the image resolution with a solid-state excitation laser

K. Irisawa*[a], T. Hirasawa[b], K. Hirota[a], K. Tsujita[a], and M. Ishihara[b]
[a] Medical Systems Research & Development Center, Research & Development Management Headquarters, FUJIFILM Corporation, 798 Miyanodai, Kaisei-machi, Ashigarakami-gun, Kanagawa, Japan 258-8538;
[b] Department of Medical Engineering, National Defense Medical College, 3-2, Namiki, Tokorozawa, Saitama, Japan 359-8513

ABSTRACT

Properties of excitation laser are the important parameters that affect the photoacoustic image quality. As for the pulse width, it is closely related to signal strength and image resolution, which reported as a result of an experiment using a laser diode that can control the pulse width easily[1]. However, though a solid-state laser is promising for a medical application due to its high pulse energy creating high photo acoustic signal, its influence on waveform or the image quality has not been discussed in detail because the pulse width is hardly changeable in a solid-state laser.

We use two kinds of solid-state lasers, i.e., Q-switched Nd:YAG and Ti-Sapphire Laser, in this study and generate different pulse width between 4.5 and 45 ns by changing wavelength and excitation energy. These laser pulses are entered into a silicon tube composed of carbon-particle suspension as absorber whose wavelength dependence for absorption is small. We detect the generated laser-induced photoacoustic waves by hydrophone.

The photoacoustic temporal waveform shows sharper as the pulse width is shorter, which also indicates high frequency signal components increase. The width of the first peak on the temporal waveform is corresponding to the pulse width. Additionally, as a result of the photoacoustic imaging experiment preformed with 192-channel PZT linear array probe to image a thin wire, the modulation transfer function shows that the narrower the pulse width, the slightly better the image resolution.

Keywords: Solid-state laser, pulse width, photoacoustic waveform, photoacoustic imaging

1. INTRODUCTION

Photo-acoustic imaging is a method for acquiring image by detecting the acoustic wave when pulsed light is incident on the light absorber.[2] The resolution performance in photoacoustic image can be better than that in optical image for the light absorber that exists in the relatively deep part of scattering objects. And also the resolution performance can be higher performed by photoacoustic imaging than by ultrasound in the imaging object that reflexes the acoustic wave and absorbs the light either.[3]
By utilizing this feature, photoacoustic imaging is promising as a functional imaging modality for clinical use in recent years. For example, Hemoglobin is a representative object in the blood that can absorb the light in living organisms, and by using photoacoustic imaging, tumors accompanied with neovascularity can be observed.[4] And by injecting the contrast medium such as pigments, the imaging of lymph vessels and lymph nodes can be observed as well.[5]

In the living organism, where is the main imaging target of photoacoustic imaging, the optical wavelengths that reachable to the depths almost without absorption is limited in the range between 650 to 1100 nm. Since the light is strongly scattered in living organism, it shall reduce significantly until it reaches the depth of body. Additionally, the conversion efficiency from optical energy to acoustic energy is low. Therefore, the high-energy pulsed light source and high-sensitivity ultrasound detector are needed for practical use.

When irradiating the pulsed light with energy density of ~20 mJ/cm^2 close to the maximum permissive exposure for the human skin and with a field of view ~1cm^2 suitable for imaging of human body, the light source is needed for producing the energy pulse higher than 20 mJ/pulse.

*kaku.irisawa@fujifilm.co.jp; phone +81 465 85-4189; fax +81 465 85-2119

Photons Plus Ultrasound: Imaging and Sensing 2012, edited by Alexander A. Oraevsky, Lihong V. Wang,
Proc. of SPIE Vol. 8223, 82232W · © 2012 SPIE · CCC code: 1605-7422/12/$18 · doi: 10.1117/12.907714

In current technology, the most practicable light source is solid-state pulse laser. With the view of determining system performance, pulse width and repetitive performance, etc. other than high energy become important when using the light source of pulse laser. As for laser pulse width, it is limited and almost fixed by properties of laser crystal, and arrangement of optical elements; it is a difficult parameter to be independently designed. Therefore, it is important to study the laser pulse width dependence of photoacoustic wave, and the effect to the image quality when uses it in imaging.

In recent years, the attempt to control the pulse width in laser diode is reported, resulting in the increase of the photoacoustic signal with the decrease of the pulse width, and the significant image blurring in the pulse width about 500 ns.[1]

The purpose of this report is to clear how much the photo-acoustic image quality is dependent on the pulse width of solid-state laser. First, it is observed the temporal waveform of photoacoustic pressure by single hydrophone with the varieties of the pulse width of excitation solid-state lasers in the range of 4.5 to 45 ns for evaluating the change of temporal waveform of photoacoustic signal depending on the pulse width in detail. Then, it is compared the temporal waveform between the experimental results and the result obtained by simplified superposition model calculation.

In addition, we acquired the photoacoustic image by using ultrasound probe array at various pulse widths to study the relations between the pulse width and image quality of photoacoustic imaging system based on US imaging systems. Finally, we evaluated the image resolution to be compared with an image resolution expected from above simplified superposition model calculations.

2. MATERIALS AND METHODS

2.1 Observation of photoacoustic temporal waveform detection

In order to generating photoacoustic wave by different laser pulse widths between 4.5 and 45ns, two kinds of *Q*-switched solid-state lasers are used as pulsed light source, that is, a Nd:YAG second harmonic generation (SHG) laser (ML-II, Minilite, Continuum Inc, USA) and a Ti-Sapphire laser (LS-2134 and LT-2211, LOTIS TII, Belarus) in which the pulse width is changed accompanied by selecting wavelength. The pulse width and wavelength from Nd:YAG SHG laser were 4.5 ns and 532 nm, respectively. In the Ti-Sapphire laser units, the pulse widths were from 14 to 45 ns at selected wavelengths from 710 to 695 nm, respectively. The laser pulse waveforms were observed by photodiode (ET-2000, Electro-Optics Technology Inc., USA), and pulse width is defined as the full width of half maximum of the pulse waveforms. The pulse energy was set around 3 mJ. Laser light is introduced via optical fiber with 600 um core diameter. As a absorber for exciting photoacoustic pressure wave, it was used a silicon tube with 0.3 and 0.4 mm inner and outer diameter, respectively, including carbon-particle suspended in water. Though the absorption of the carbon-particle suspension is changed by the wavelength change, its absorption change is relatively small by a factor of around 0.7 in the range of wavelength from 532 to 720 nm as shown in the inset of figure 1(*a*). The mean diameter of carbon particles in water suspension was 200 nm.

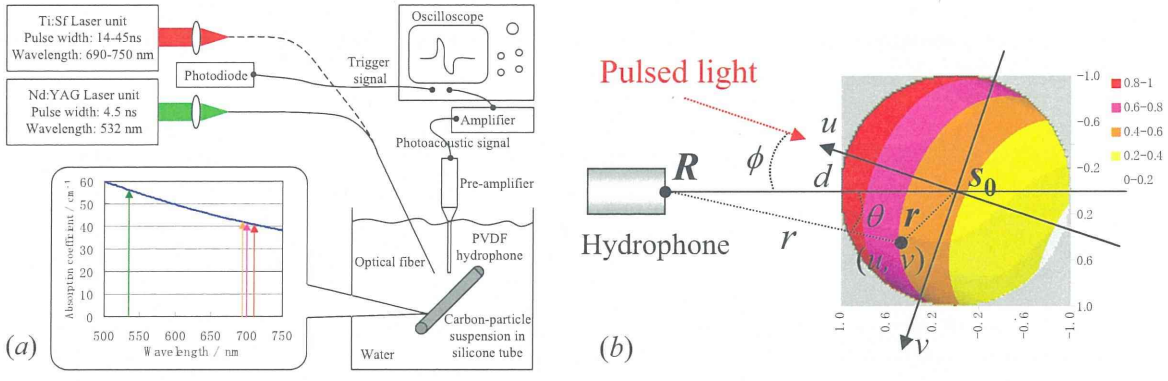

FIG. 1. (*a*) Experimental set up for observing photoacoustic waveforms. The inset shows the wavelength dependence of absorption coefficient for carbon-particle suspension, together with the wavelength used to change pulse width.

FIG. 1. (*b*) Relation between the coordinates systems used in calculation model and an example of absorption distribution *A* calculated with the parameters, $a = 0.3$ mm, $d = 5.0$ mm, $r_P = 1.0$ mm, $\mu = 5.62$ cm^{-1}, $\phi = 25$ deg.

Photoacoustic wave is detected by PVDF needle hydrophone (HPM02/1, Precision Acoustics Ltd., UK) with 0.2 mm element diameter and observed by oscilloscope. The angle between the PVDF needle hydrophone and laser incident direction was 25 degrees. The distance between silicon tube and hydrophone is set to 5 mm.

2.2 Theoretical model and numerical calculation of photoacoustic temporal waveform

The simple calculation model is introduced to consider the influence of pulse width and absorption distribution change simultaneously caused by wavelength change of laser pulse. The photoacoustic wave generated from the tube is calculated as a superposition of the spherical photoacoustic wave that generated from the individual carbon-particle of different spatial location with considering the concentration distribution of carbon-particle and distribution of incident light.

The reached photoacoustic pressure $p_{\mathrm{micro}}(\boldsymbol{R}, t)$ in observation point $\boldsymbol{R}$ on time t from a microparticle located in $\boldsymbol{r}$ is obtained as spherical wave proportional to the temporal differential waveform of light pulse, and expressed as,[6, 7]

$$p_{micro}(\boldsymbol{R},t)=\frac{k}{|\boldsymbol{r}-\boldsymbol{R}|}\frac{d}{d(t-\frac{|\boldsymbol{r}-\boldsymbol{R}|}{v_s})}I(t-\frac{|\boldsymbol{r}-\boldsymbol{R}|}{v_s}) \tag{1}$$

Where, I is the temporal waveform of intensity of excitation laser pulse, and k is the coefficient related with conversion efficiency from the laser pulse to acoustic wave, and v_s is the sound speed. Such expression is considered to be satisfied in the case of certain particle that arises uniform thermal expansion derived from uniform absorption distribution or momentary heat diffusion in the particle. The carbon-particle with 200 nm of mean hydrodynamic diameter is used in the experiment, which is also assumed to be satisfied as the below expression.

Then, the pressure waveform $p_{\mathrm{macro}}(\boldsymbol{R}, t)$ from the carbon-particle suspension inside the tube is assumed to be formed as superposed waveform of p_{micro} from each particle in different locations. The absorption distribution of carbon-particle suspension is defined as $A(\boldsymbol{r}\text{-}\boldsymbol{R})$. Therefore, $p_{\mathrm{macro}}(\boldsymbol{R}, t)$ is expressed as below.[8]

$$\begin{aligned}
p_{macro}(\boldsymbol{R},t) &= \iiint A(\boldsymbol{r}-\boldsymbol{R})\times\frac{k}{|\boldsymbol{r}-\boldsymbol{R}|}\frac{d}{d(t-\frac{|\boldsymbol{r}-\boldsymbol{R}|}{v_s})}I(t-\frac{|\boldsymbol{r}-\boldsymbol{R}|}{v_s})dV \\
&= \int_0^{\pi}\int_{-\frac{\pi}{2}}^{\frac{\pi}{2}}\int_0^{|\boldsymbol{r}-\boldsymbol{R}|=v_s t}\frac{kA(\boldsymbol{r}-\boldsymbol{R})}{|\boldsymbol{r}-\boldsymbol{R}|}I'(t-\frac{|\boldsymbol{r}-\boldsymbol{R}|}{v_s})|\boldsymbol{r}-\boldsymbol{R}|^2\sin\theta d|\boldsymbol{r}-\boldsymbol{R}|d\theta d\varphi \\
&= \int_0^{|\boldsymbol{r}-\boldsymbol{R}|=v_s t}\frac{k}{|\boldsymbol{r}-\boldsymbol{R}|}\int_0^{\pi}\int_{-\frac{\pi}{2}}^{\frac{\pi}{2}}A(\boldsymbol{r}-\boldsymbol{R})dS\times I'(t-\frac{|\boldsymbol{r}-\boldsymbol{R}|}{v_s})d|\boldsymbol{r}-\boldsymbol{R}| \\
&= \left[\frac{k}{|\boldsymbol{r}-\boldsymbol{R}|}\int_0^{\pi}\int_{-\frac{\pi}{2}}^{\frac{\pi}{2}}A(\boldsymbol{r}-\boldsymbol{R})dS\right]*\left[I'(t-\frac{|\boldsymbol{r}-\boldsymbol{R}|}{v_s})\right]
\end{aligned} \tag{2}$$

That is, the observed pressure waveform can be expressed by the convolution of integrated $A(\boldsymbol{r}\text{-}\boldsymbol{R})$ and temporal differentiation of pulse intensity.

$A(\boldsymbol{r}\text{-}\boldsymbol{R})$ is a function of incident light and absorber distribution. In the present model, it is assumed that the light is collimated light with Gaussian spatial distribution, and the concentration of carbon-particle inside of the tube is uniform, as well as the exponential decay of light intensity from the incident interface between the tube and the suspension to the traveling direction on each cross-section of the tube. For convenience of calculation, $A(\boldsymbol{r}\text{-}\boldsymbol{R})$ is calculated according the positional coordinates (u, v, w) whose origin is set at the tube center $\boldsymbol{s}_0$. The direction of u and w are corresponded with the light incident direction and a longitudinal direction, respectively. The angle ϕ between u direction and observation direction $(\boldsymbol{s}_0\text{-}\boldsymbol{R})$, tube radius a, the distance d between the tube center and detector, and absorption coefficient μ of carbon-particle suspension is variable, which are determined from the experimental arrangement or condition. The coordinate conversion between (r, φ, θ) and $(u, v, w)$was driven as a below expression (3), and A(u, v, w) is given as expression (4). And also, an example of calculation result of A(u, v, w) is shown in figure 1(b).

$$\begin{pmatrix} u \\ v \\ w \end{pmatrix} = R(-\phi)\cdot\{(\boldsymbol{r}-\boldsymbol{R})-\boldsymbol{s}_0+\boldsymbol{R}\} = \begin{pmatrix} \cos\phi & \sin\phi & 0 \\ -\sin\phi & \cos\phi & 0 \\ 0 & 0 & 1 \end{pmatrix}\begin{pmatrix} d-r\cos\theta\cos\varphi \\ -r\sin\theta \\ r\cos\theta\sin\varphi \end{pmatrix} \tag{3}$$

$$A(u,v,w) = \exp\left\{-\mu\left(\sqrt{a^2-v^2}-u\right)\right\}\cdot\exp\left(-\frac{2\left(v^2+w^2\right)}{r_P{}^2}\right), u^2+v^2 \le a^2 \tag{4}$$

From these expressions, the temporal photoacoustic waveforms generated by laser pulse with various pulse widths were calculated. In the calculation, laser pulse waveform $I(t)$ was assumed to be a Gaussian function, and its full width of half maximum was defined as pulse width.

In addition to obtain the calculated temporal waveform after the hydrophone detection, the frequency components of the calculated temporal waveform was multiplied by the frequency response of hydrophone based on its calibration data and specifications (+/-4 dB < 35 MHz), followed by computing the inverse Fourier transform.

2.3 Evaluation of photoacoustic image acquired with ultrasound array probe

In order to discuss the influence of pulse width on image quality, photoacoustic images of thin carbon wire were acquired by using practical ultrasound array probe at various laser pulse widths. Then, Modulation Transfer Function (*MTF*) that is one of the evaluation indexes of image resolution was computed from each PA image.

The same solid-state lasers mentioned in 2.1 section were used as pulsed light sources. Pulse laser light was transferred by optical fiber for illuminating the thin 0.124 mm diameter carbon wire. The carbon wire was perpendicularly arranged with array direction of the array probe. The photoacoustic wave was detected by the array probe which was constructed of 192 channels of PZT transducers with 0.3 mm channel pitch. The center frequency of transducers was 8 MHz. Output signals of transducers were A/D converted with 25 ns sampling interval, and preprocessed in PAI system[2]. The images were acquired in each 0.02 mm movement of the array probe for sampling more finely than channel pitch, by using motorized stage scanning parallel to the array direction. After reconstructing the photoacoustic image by Fourier transform algorism,[8] followed by obtaining the amplitude signal by Hilbert transformation, the two-dimensional point spread function was obtained. *MTF*s of the array and depth directions were computed from the point spread functions by Fourier transform of data line along the array and time directions, respectively.

3. RESULTS AND DISCUSSIONS

3.1 Comparison of temporal waveforms between experiment and calculation

In figure 2 (*a*), it is shown that the photoacoustic signal waveforms detected with the needle hydrophone for a above mentioned tube phantom at various excitation laser pulse width from 4.5 to 45 ns, which are normalized at positive peaks. In each waveform, a strong positive peak appears initially, and then the broad negative peak appears. The time interval between positive and negative peak in each waveform is about 200 ns, which are in accordance with the inner tube diameter of 0.3 mm considering the sound speed of 1500 m/s. It is observed that the widths of positive peak increases and the negative peak become strong with increasing the laser pulse width. In figure 2 (*b*), the frequency spectra of the photoacoustic waveforms at various excitation laser pulse width is shown, which are normalized at in the frequency of 2 MHz. For each spectrum, the amplitude value is gradually decreased as frequency increases. The high-frequency components become large with narrowing laser pulse, and the signal remains up to 40 MHz in 4.5 ns pulse width.

To compare between the experimental and model calculated photoacoustic waveform, calculation results of photoacoustic temporal waveform before (as-reached) and after hydrophone detection are shown in figure 3 (*a*) and (*b*), respectively. The shape and the pulse width dependence of calculated waveforms before the hydrophone detection exhibit almost the same tendency according to the experimental waveforms. Furthermore, the calculated waveforms are broadened by considering the hydrophone detection, and demonstrate more close similarities to experimental waveforms.

The similar waveforms were obtained from both experiment and calculation, indicating that the influence of excitation-laser pulse width on photoacoustic signal is almost be able to explained on the basis of the simple model, that is, the

observed photoacoustic waveform is given by the superposition of photoacoustic waveforms from micro particles. In the condition of the present study, so the laser pulse width and the transit time of photoacoustic wave in the absorber are close in order, the above-described change is observed in shape of waveform. In case that the laser pulse width is enough smaller than the transit time of photoacoustic wave in the absorber, the sharp peak at the boundary of absorber appears in the temporal photoacoustic waveform. And also, when the laser pulse width is enough larger than the transit time of photoacoustic wave in the absorber, the photoacoustic waveform is approximately proportional to the time derivative of laser pulse intensity.

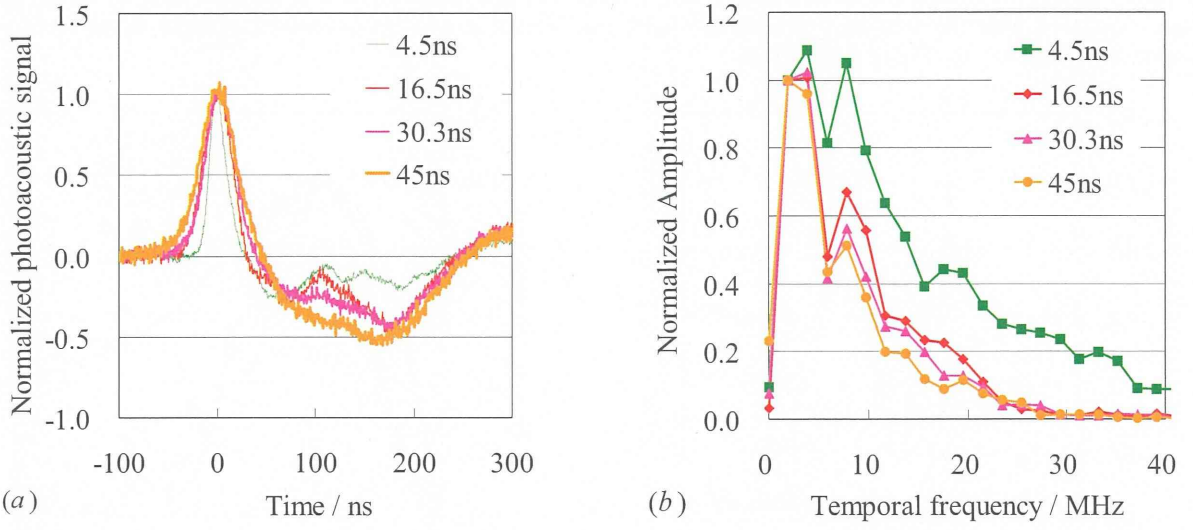

FIG. 2. (*a*) Observed temporal waveforms of photoacoustic signal and (*b*) their frequency spectra at various pulse widths.

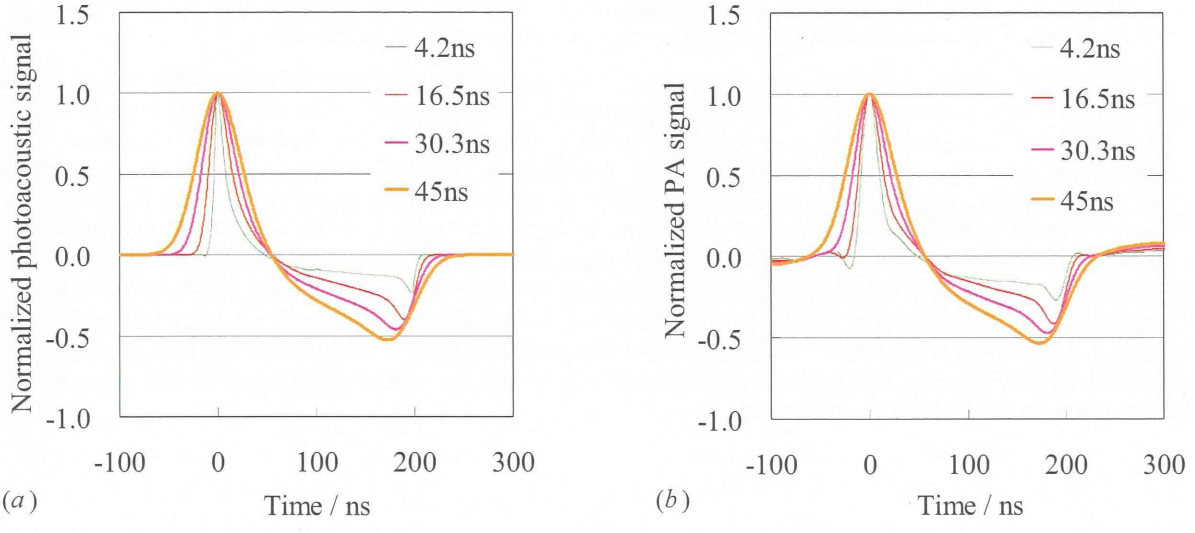

FIG. 3. (*a*) Calculated as-reached temporal waveform before hydrophone detection and (*b*) calculated temporal waveform under consideration of hydrophone frequency response.

3.2 Imaging with ultrasound array probe

The photoacoustic signal shows the wide-band frequency spectrum dependent on laser pulse width when detecting with wide-band probe such as PVDF hydrophone. On the other hand, it is generally used a practical narrow-band PZT array probe in acquiring image. In figure 4 (*a*), it is shown the photoacoustic temporal waveforms, which is intended to study the pulse width dependence of image quality when detected with the PZT probes mentioned above. It is also shown that the as-reached temporal waveform which is calculated by the above superposition model. However, the observed waveforms are quite different with the calculated one, and the change of temporal waveform corresponding with pulse width is not clearly observed. As is shown in figure 4(*b*), frequency profiles detected with the PZT array probe are lowly limited, compared with the frequency profile of model calculation. It was also observed a slight decrease in peak frequency with broadening of laser pulse width.

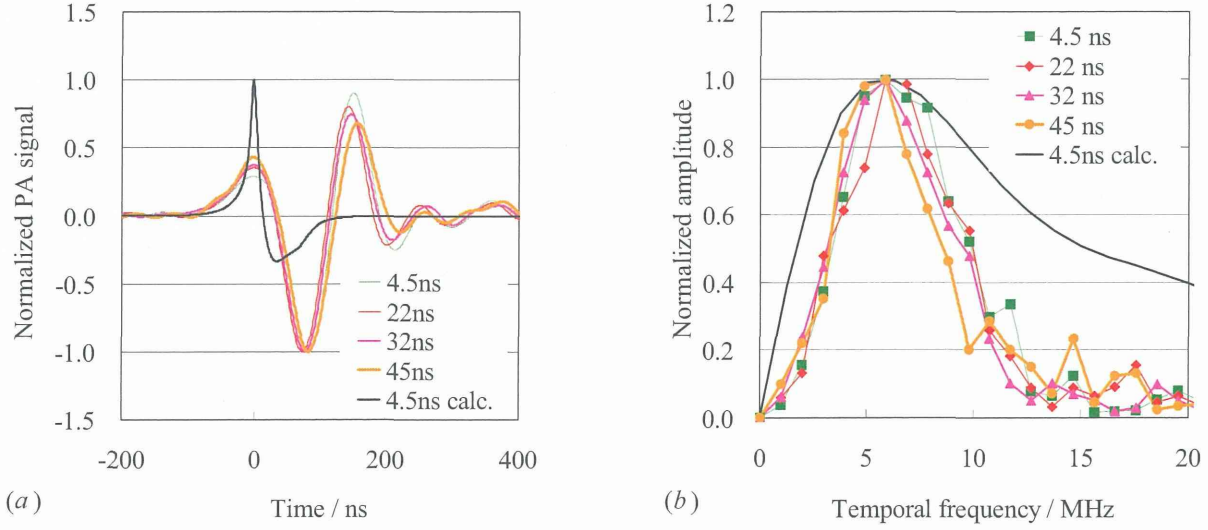

FIG. 4. (*a*) Temporal waveforms of photoacoustic signal detected by PZT array probe and (*b*) their frequency spectra of at various pulse widths, together with the calculated as-reached waveform at 4.5 ns pulse width.

To study the influence of the small shift of peak frequency on image quality caused by the pulse width change, the Point Spread Function (*PSF*) from the pressure amplitude image and Modulation Transfer Function (*MTF*) for both depth and array directions were examined, as shown in figure 5 (*a*) and (*b*), respectively. It was observed a slight increase of *MTF* in the spatial frequency around 3 mm^{-1} with pulse-width narrowing for the depth direction. For the array direction, the influence of pulse width change on *MTF* is hardly observed, since the *MTF* in high spatial frequency is suppressed due to the blurring occurred by the PZT-element pitch of 0.3 mm. In figure 6 (*a*) and (*b*), it shows the *PSF* and *MTF* obtained from the calculated as-reached photoacoustic waveform of depth direction with consideration of experimental conditions in image acquiring. From these calculated results, it is indicated that the change of laser pulse width influences *PSF* and *MTF*, especially, for the high spatial frequency side. However, the signals such like the above spatial frequency cannot be obtained and there was small impact on image quality when the existing practical narrow band probe was used. For the needs of high resolution for diagnosis, probe band and pulse width are expected to give great impact on the image resolution, which should be taking into account.

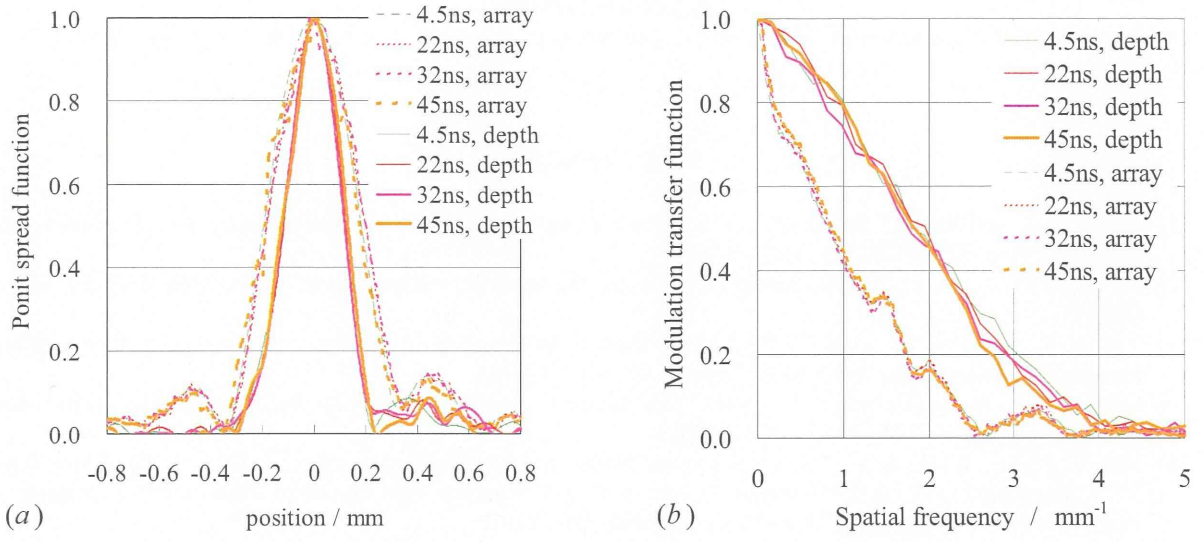

FIG. 5. (*a*) *PSF* and (*b*) *MTF* from the images acquired by PZT array probe.

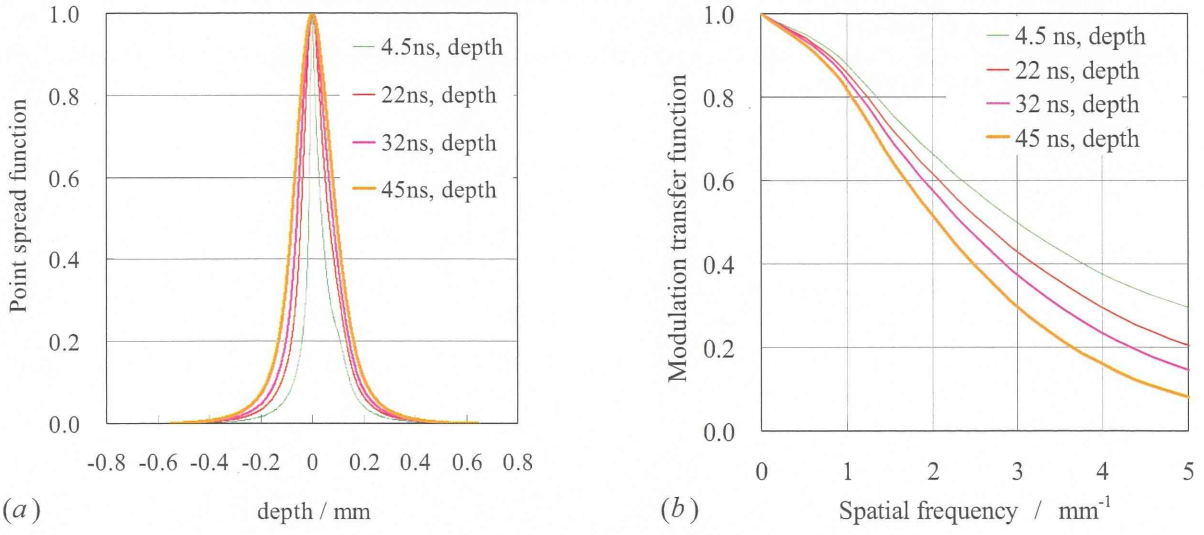

FIG. 6. (*a*) *PSF* and (*b*) *MTF* from the model calculation of as-reached photoacoustic waveforms.

4. CONCLUSIONS

The temporal waveforms are significantly influenced by change of the laser pulse width from 4.5 to 45 ns, when those are generated by a solid-state laser pulse and observed by the wide-band detector like a hydrophone.

Such changes of waveforms can be qualitatively explained by a simple model that the observed waveform is given by superposition of the photoacoustic waveform from microparticles which is proportional to the temporal derivative of light pulse. Furthermore, better correspondence between calculated and observed results is obtained by taking into account the effect of frequency filtering due to the frequency response of hydrophone.

Though the wide-band frequency components are essentially included in photoacoustic signal, the influence of the laser pulse width on the image resolution is substantively small when photoacoustic signal are detected by the narrow-band practical ultrasound probe with the center frequency of 8 MHz. However, it is expected to take into account the effect of the pulse width on image resolution in the case of using a wider-band or higher-frequency probe.

Acknowledgement

This work was partially supported by Health and Labor Sciences Research Grants for Research on Medical Device Development.

REFERENCES

[1] Allen, T. J. and Paul C. Beard, P. C., "Dual wavelength laser diode excitation source for 2D photoacoustic imaging," Proc. SPIE 6437, 64371U1-9 (2007).
[2] Li, C and Wang, L. V., "Photoacoustic tomography and sensing in biomedicine," Phys. Med. Biol. 54, R59-97, (2009).
[3] Tsujita, K., Ishihara, M., et al., "Effect of the illumination method on photo-acoustic image quality with array transducer based system," Proc. SPIE 7899, 78992W1-6 (2011).
[4] Oraevsky, A. A., Savateeva, E. V., et al., "Optoacoustic imaging of blood for visualization and diagnostics of breast cancer," Proc. SPIE 4618, 81-94 (2002).
[5] Kim, C., Song, K. H., et al., "Sentinel Lymph Nodes and Lymphatic Vessels: Noninvasive Dual-Modality in Vivo Mapping by Using Indocyanine Green in Rats-Volumetric Spectroscopic Photoacoustic Imaging and Planar Fluorescence Imaging," Radiology 255, 442-450 (2010).
[6] Calasso, I. G, Craig, W., and Diebold, G. J., "Photoacoustic Point Source," Phys. Rev. Lett. 86, 3550-3553 (2001).
[7] Diebold, G. J., Sun, T., and Khan, M. I., "Photoacoustic Monopole Radiation in One, Two and Three dimensions," Phys. Rev. Lett. 67, 3384-3387 (1991).
[8] Wang, W., Xing, Da., Zeng, Y. and Chen, Q., "Photoacoustic imaging with deconvolution algorithm," Phys. Med. Biol. 49, 3117-3124 (2004).

日本光学会年次学術講演会

Optics & Photonics Japan 2011

— Osaka —

開催のお知らせ

開催日：2011年11月28日(月)~30日（水）

会　場：大阪大学 コンベンションセンター・体育館（大阪府吹田市山田丘1-1）

主　催：社団法人応用物理学会 分科会　日本光学会

共　催：大阪大学 フォトニクス先端融合研究拠点

大阪大学 光科学センター

◆　おもな日程（予定）　◆

講演申込期間：2011年7月1日（金）～8月5日（金）

ポストデッドラインペーパー投稿：2011年10月3日（月）～10月21日（金）

事前参加登録期間：2011年7月1日（金）～10月31日（月）

協賛学協会※の会員にも一般講演応募資格があります（※応用物理学会，電子情報通信学会など，詳しくは「光学」6号およびOPJ2011ホームページ参照）.

◆　問い合わせ先　◆

Optics & Photonics Japan 2011 事務局

〒164-0003　東京都中野区東中野4-27-37　株式会社アドスリー内

TEL 03-5925-2840　FAX 03-5925-2913

E-Mail：opj@opt-j.com　URL：http://www.opt-j.com/opj2011/

P65

光音響画像化技術の要素技術開発とシステム化：動物モデルによる性能検証

Development and integration of photoacoustic imaging technology: animal model demonstration

平沢　壮[1)]，○石原美弥[2)]，藤田真敬[3)]，北垣　学[4)]，大谷直樹[5)]，菊地　眞[6)]
Takeshi Hirasawa[1)], ○Miya Ishihara, Ph.D.[2)], Masanori Fujita, M.D., Ph.D.[3)], Manabu Kitagaki, M.D.[4)], Naoki Otani, M.D., Ph.D.[5)], Makoto Kikuchi, Ph.D.[6)]

防衛医科大学校医用工学講座[1) 2) 4)]，防衛医科大学校防衛医学研究センター異常環境衛生研究部門[3)]，防衛医科大学校脳神経外科学講座[5)]，防衛医科大学校教育担当副校長，医学教育部長[6)]
Department of Medical Engineering, National Defense Medical College[1) 2) 4)], Division of Environmental Medicine, National Defense Medical College Research Institute[3)], Department of Neurosurgery, National Defense Medical College[5)], National Defense Medical College, Vice President & Dean[6)]
E-mail:miyaishi@ndmc.ac.jp

Photoacoustic imaging is a technique combined with optical and ultrasound methods. Here we report the development of a photoacoustic imaging system for animal experiments with the aim of searching its clinical value.

1．光音響画像化技術

光音響画像化技術 (Photoacoustic imaging technology)は，2010 年 2 月の Nature の分子イメージング特集(1)の中で PET, MRI, 光などのモダリティと並んで独立したモダリティとして紹介され，さらに NCI (National Cancer Institutes)ではトランスレーショナルリサーチ（基礎医学研究の成果を診断・治療の形で臨床の場に橋渡しする研究）の大型研究プロジェクトが立ち上がるなど，新しい分子イメージング技術、画像診断技術として世界的に着目されている。

光音響画像化原理は，光の吸収体で発生した音響波の伝搬時間（センサまでの到達時間）から光の吸収体の位置情報や信号強度より吸収係数に関する情報を断層画像にするもので，光と生体の相互作用を画像化する技術の１つである。光の吸収体で音響波が発生するには，吸収されたレーザ光のエネルギーによる加熱領域が熱膨張し，周囲と異なる温度分布（密度分布）が生じることで応力閉じ込め（stress confined）条件、つまり，熱弾性過程により応力波（光音響波）が発生する。熱弾性効果による応力波発生は，光のパラメータを適当に設定することで特定の吸収体を選択的に励起可能（例えば血液に吸収する波長を励起光に選択する）で，発生する応力波の時間的挙動を制御することにより、応力波発生源の位置情報だけではない特徴抽出の可能性を持つ。

光音響画像は用途に応じて表１のようにいくつかの方式に分類される。

Table1 Classification and application of photoacoustic imaging

PAI: Photoacoustic imaging(2)	汎用的　→　臨床向き
High Frequency PAI(3)	小動物用
PAT: Photoacoustic tomography(4)	小動物用
PAM: Photoacoustic microscopy(5)	顕微鏡応用
Intravascular catheter(6, 7)	経カテーテル、内視鏡

共通した主要な要素技術として，<1>光音響波発生励起源である光源及びその導光技術，<2>光音響波の検

出のためのセンサ技術，<3>検出した信号から画像を構築する画像再構成処理技術，が挙げられる。これらの要素技術を用途別に開発し仕様を決めて、各々システム化している。

２．構築している臨床価値探索用システム

我々は、造影剤を使用しない，生体由来の信号であるヘモグロビンを吸収体とした光音響画像の臨床価値を探索することを目的としてPAI型システムを構築した。このシステムでは、種々の動物（ウサギ、ラット、マウス）の病態モデルを対象に光音響画像が取得できるように，光源やセンサ，及びそれに応じたデータ取得及び画像再構成処理が設定できるようになっている。その構成を図１に示す。以下、要素技術ごとにシステムについて記述する。

<1>光源：生体内の光吸収体の光特性で応力閉じ込め条件を満たすにはパルス幅がナノ秒程度の光源，かつその波長は生体の分光的窓である近赤外が一般的である。我々は連続的に波長を変えられる市販のTi:Sapphireレーザ，Nd:YAGレーザの第2高調波，及びOPOを用途に応じて使用し，いずれも石英ガラスファイバーを用いて画像化対象まで導光できるようにしている。

<2>センサ：センサ材料には圧電素子を使用する。我々は超音波診断で一般的に使用されているPZT素子に加えて広帯域な周波数特性を持つP(VDF-TrFE)素子を用い，多チャンネル化したセンサと導光用光ファイバーと一体化させて使用している。多チャンネルセンサをスキャンして複数の観測点で音響波を観測することで三次元画像化を可能としている。

<3>画像再構成処理：センサで検出した信号の多チャンネル同時取り込み（最大 64ch）及び信号増幅、かつ高速ADC変換が可能で，励起用パルスレーザと同期及び信号処理及び表示用PCにデータ転送が出来るようになっている。さらに，光音響画像と超音波画像との重畳が可能である。現在までに、画像表示までほぼリアルタイムの性能(<1.5秒/frame)が得られているため、体動の影響を軽減して画像化できるようになっている。

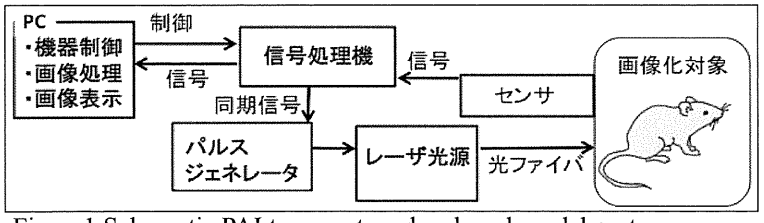

Figure1 Schematic PAI type system developed our laboratory

図１に示すPAI型システムを用いて、現在までにマウスの大腿動脈と静脈の血管画像やその酸素飽和度マッピングが可能であることを確認した。

参考文献

(1) M. Baker, " Whole-animal imaging: The whole picture", Nature, 463 (7283), pp. 977-980 (2010)
(2) K. Chulhong et al., "Deeply penetrating in vivo photoacoustic imaging using a clinical ultrasound array system", Biomed. Opt Exp, 1(1), pp278-284, (2010)
(3) Visual Sonics 社ホームページ, http://www.visualsonics.com/
(4) L. Meng-Lin, et al., "Simultaneous molecular and hypoxia imaging of brain tumors in vivo using spectroscopic photoacoustic tomography", Proc. IEEE, 96(3), pp.481-489, (2008)
(5) F. P. Christopher, et al., "In vivo functional photoacoustic microscopy of cutaneous microvasculature in human skin", J. of Biomed. Opt, 16(2), pp.026004, (2011)
(6) A. B. Karpiouk, et al., "Development of a catheter for combined intravascular ultrasound and photoacoustic imaging", Rev. Sci. Instrum, 81, pp.014901, (2010)
(7) S. Sethuraman, et al., "Spectroscopic intravascular photoacoustic imaging to differentiate atherosclerotic plaques", Opt. Exp., 16(5), pp.3362-3367, (2008)

謝辞

本研究の一部は平成 23 年度厚生労働省研究費補助金（医療機器開発推進研究事業）（H23-医療機器-一般005）の助成を受け実施された。

本研究を遂行するにあたり、富士フイルム株式会社の辻田和宏氏、広田和弘氏、入澤 覚氏に謝意を表する。

Photoacoustic Measurement Technology in Regenerative Medicine of Articular Cartilage

Miya Ishihara[1], Masato Sato[2], Toshiharu Kutsuna [2], Joji Mochida [2], Makoto Kikuchi [1]
[1]Department of Medical Engineering, National Defense Medical College
[2]Department of Orthopaedic Surgery, Tokai University School of Medicine

Abstract: We developed a measurement method of viscoelastic property using photo-acoustic temporal waveform and extracellular matrix characterization using time-resolved auto-fluorescence spectroscopy. The viscoelastic properties enabled to be determined and the status of extracellular matrix formation enabled to be provided when engineered articular cartilage cultured for various periods were used as samples. We demonstrated possibility of monitoring of the repair process after transplantation and diagnosis of a disease before regenerative medicine.

Keywords: articular cartilage, viscoelastic property, extracellular matirix

1. Introduction

There is a demand in the field of regenerative medicine of articular cartilage for noninvasive measurement technology that enables determination of functions and components of engineered tissue.

As the major function of articular cartilage is viscoelastic property, the photoacoustic measurement method may be a strong candidate for the required technology.

Extracellular matrix of articular cartilage is responsible for the major functional properties of cartilage. Consequently, characterization of extracellular matrix should be performed.

To meet this demand, we developed a measurement method of viscoelastic property using photo-acoustic temporal waveform and extracellular matrix characterization using time-resolved auto-fluorescence spectroscopy.

2. Photoacoustic measurement and autofluorescence measurement

We discovered that stress wave propagation and attenuation by pulsed laser irradiation influenced tissue viscoelasticity, and based on this principle, proposed the use of photoacoustic measurement for viscoelastic characterization of biological tissue [1-2]. As the major function of articular cartilage is viscoelastic property, the photoacoustic measurement method may be a strong candidate for the required technology [3-5].

Extracellular matrix of articular cartilage is responsible for the major functional properties of cartilage. Consequently, characterization of extracellular matrix should be performed for evaluation of regenerative medicine for articular cartilage. Articular cartilage is composed of scattered chondrocytes embedded in an abundant extracellular matrix. The matrix is mainly composed of proteoglycans and type II collagen, which consists of endogenous biomolecules. Fluorescence measurement can provide information about endogenous fluorescent biomolecules.

3. Results and discussion

The viscoelastic properties enabled to be determined by the photoacoustic method when engineered articular cartilage cultured for various periods (up to 12 weeks) were used as samples. The photoacoustic measurement was also revealed to provide information about the status of extracellular matrix formation during cultivation. In vivo photoacoustic measurements were demonstrated to verify the usefulness for repeated measurement of viscoelastic properties in order to evaluate the process of regeneration after transplantaion tissue-engineered cartilage. About a 40% difference between the viscoelasticity of allografted engineered cartilage that of surrounding native tissue was shown just after surgery. The difference was significantly reduced at 4 and 12 postoperative weeks. Therefore, since the photoacoustic measurement method enables assessment of the progress of restoration of the viscoelasticity of articular cartilage, its main function, this method would be useful as an evaluation method in regener.

There were significant differences in the measured fluorescent parameters among the culture conditions of cartilage because chondrocytes produce a specific extracellular matrix depending on its culture condition. The constituents of the extracellular matrix of hyaline cartilage are different from those of the extracellular matrix of fibrous cartilage. Discrimination of hyaline cartilage and fibrous cartilage enables characterization of the regenerated articular cartilage because one of the serious problems in regenerative medicine of articular cartilage is that repaired osteochondral defect using tissue-engineering technology should be regenerated as hyaline cartilage, however it has been often regenerated as fibrous cartilage.

4. Conclusion

We developed the measurement method for the evaluation of the viscoelastic properties by the photoacoustic method and characterization of the extracellular matrix of tissue engineered cartilage by the time-resolved auto-fluorescence spectroscopy. Both of them are expected to become a useful evaluation method in regenerative medicine of articular cartilage.

Reference

1. Ishihara M, et al., Jpn J Appl Phys 42:556-558 (2003).
2. Ishihara M, et al., Proc of SPIE 4961:221-226(2003).
3. Ishihara M, et al., Tissue Engineering 11(7-8):1234-1243 (2005).
4. Ishihara M, et al., The review of laser engineering 32(10):640-644 (2004).
5. Ishihara M, et al., Lasers in Surg. & Med.:38:249-255 (2006).

深部組織の高分解能画像化に向けた光音響画像診断法の開発と評価

平沢壮[1], 石原美弥[1], 辻田和宏[2], 入澤覚[2], 北垣学[1], 藤田真敬[3], 菊地眞[1]
[1]防衛医科大学校　医用工学講座
[2]富士フイルム株式会社　R&D 統括本部　メディカルシステム開発センター
[3]防衛医科大学校　防衛医学研究センター　異常環境衛生研究部門

Development and evaluation of photo-acoustic imaging method for high resolution deep tissue imaging

Takeshi Hirasawa[1], Miya Ishihara[1], Kazuhiro Tsujita[2], Kaku Irisawa[2], Manabu Kitagaki[1], Masanori Fujita[3], Makoto Kikuchi[1]
[1]Department of Medical Engineering, National Defense Medical College
[2]FUJIFILM Corporation Research and Development Management Headquarter, Medical Systems Research and Development Center
[3]Division of Environmental Medicine, National Defense Medical College Research Institute

Abstract: Photo-acoustic imaging (PAI) is an emerging functional imaging method, in which, optical absorbers in biological tissue such as hemoglobin are illuminated by nanosecond pulse laser to produce ultrasounds then, ultrasounds are detected by piezoelectric sensors to form a tomography. Although PAI can provide high resolution image at depth exceeding the limitation of conventional optical techniques, the penetration depth is restricted by both optical scattering and acoustic attenuation, and the resolution is restricted by specifications of acoustic sensor such as directionality, frequency band width, and aperture. In this research, penetration depth and resolution of PAI were experimentally analyzed. Furthermore, PAI of arteriolar phantoms placed in highly optical scattering ambient medium was demonstrated to show the validity of this method. As a result, arteriolar phantoms placed few centimeters away from detector surface were imaged in sub-millimeter resolution. Clinical application for superficial organs and vascular could be considered.
Keywords: Photoacoustic, Optoacoustic, Thermoacoustic, Medical Imaging, Ultrasound, P(VDF-TrFE),

1. Introduction

Photo-acoustic imaging (PAI) is a relatively new diagnostic imaging technique using photo-acoustic (PA) effect. In PA effect, optical absorbers in biological tissue illuminated by pulsed laser generate ultrasounds due to thermo-elastic expansion [1]. Ultrasounds produced by optical absorbers propagate through biological tissue and then, detected by acoustic sensor consists of piezoelectric elements. The distance between an optical absorber and an acoustic sensor can be calculated from arrival time of signal. Furthermore, PA image which reflects optical properties of tissue can be obtained from PA signals measured at multiple positions. By scanning single sensor or using array sensor with multiple elements, those signals can be obtained.

PAI can provide high resolution image at depth exceeding the limitation of conventional optical imaging techniques which detect reflected or transmitted light, since ultrasound scattering is two to three orders of magnitude weaker than optical scattering in biological tissue [1]. Furthermore, PAI can provide not only anatomical, but also tissue characteristic and functional information by using optical property of tissue which can be extracted from PA signals. Taking advantage of these merits, medical applications were reported for example, functional imaging of brain [2] and high resolution imaging of superficial vascular [3].

Our goal is clinical application of PAI. In order to find the appropriate target to image, limitations of penetration depth and image resolution should be verified. In PAI, optical scattering and acoustic attenuation limits penetration depth. In this study, we experimentally evaluated penetration depth and resolution.

2. Material and Method

In order to evaluate penetration depth of PAI, we experimentally verified the depth of detection limit. In this experiment, phantoms placed in optical scattering material were imaged. We also evaluated the depth dependence of image resolution.

A schematic diagram of PAI system is shown in Fig.1. Second harmonic generation of Q-switched Nd;YAG laser (Minilite II, Continuum) with wavelength of 532 nm was used as excitation laser pulse. Repetition rate and full width half maximum (FWHM) of laser pulse were 10 Hz and 3-4ns, respectively. The laser was focused onto an end of optical fiber and then, guided to phantoms.

Our original acoustic sensor made of piezo-electric copolymer film P(VDF-TrFE) detected ultrasound. The size of rectangular shaped sensor element was 0.5 × 6.0 mm^2. P(VDF-TrFE) has relatively wide frequency band comparing to piezo-electric ceramic PZT which is widely used for ultrasonography probe [4]. Since P(VDF-TrFE) sensed most of frequency components of ultrasound induced by PA effect, information regarding to generation and propagation of ultrasound could be extracted from waveform. FET amplifier (SA-220F5, NF Electronic Instruments, 46dB, 0.1 - 80 MHz) amplified PA signal detected by acoustic sensor then, the oscilloscope measured the amplified signal. In order to obtain PA image, acoustic signals were measured at multiple positions by scanning acoustic sensor in direction horizontal to surface of sensor element using motorized stage.

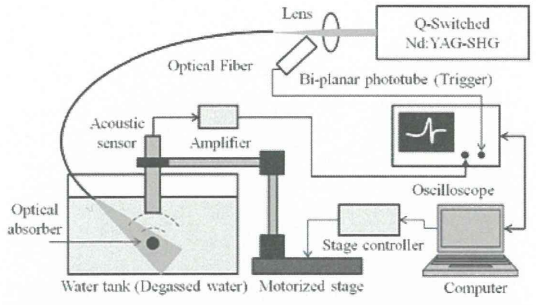

Fig. 1 Schematic diagram of experimental apparatus

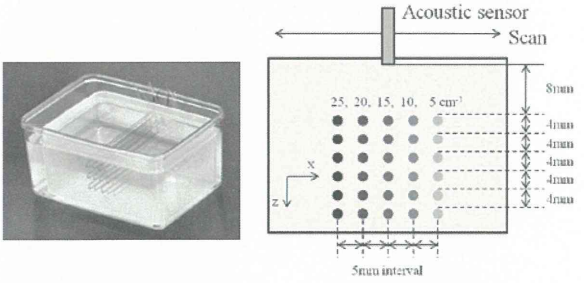

Fig.2 Arteriolar phantoms and schematic of its profile

Arteriolar phantoms made of silicon tube (inner diameter 0.5mm, outer diameter 0.6mm) filled with diluted black ink were imaged in this experiment. Optical absorption coefficient μ_a of phantoms could be adjusted by density of ink. Phantoms with different absorption coefficients were placed in arrangement shown in Fig.2. By imaging phantoms shown in Fig.2, the depth of detection limit could be clarified. The phantoms were placed in mixed medium of degassed water and optical scatterer (Intralipos). Scattering coefficient μ_s of ambient medium was adjusted by density of optical scatterer [5]. Since usage of near-infrared (NIR) light with deep penetration in biological tissue was preferred for clinical application, the reduced scattering coefficient μ_s' is adjusted to the value of muscle for NIR light [6].

In this experiment, the energy of laser pulse at the output of an optical fiber was adjusted to 6 mJ/pulse. The energy density less than damage threshold of biological tissue (ANSI safety limit: 20 mJ/cm^2) could be achieved by expanding diameter of laser beam. PA signals were measured at multiple measurement positions by scanning acoustic sensor 200 times with step of 0.2 mm. In order to enhance the signal to noise ratio, the signals were averaged 4 times. Image reconstruction algorithm was applied for signals measured at 200 positions to form a tomography.

3. Results and Discussion

As a result of experiment, the phantom with μ_a of 25 cm^{-1} was detected at a depth of 28 mm. However, image intensity decreased with μ_a. In case of μ_a =5 cm^{-1}, the intensity decreased to noise level at a depth of 20 mm. Although the absorption coefficient of blood in NIR depended on wavelength of laser and oxygen saturation, it was approximately 5-10 cm^{-1}. Therefore, the blood vessel at depth of 20-24mm could be imaged in this condition. Increase of laser pulse energy or use of optical contrast agents can increase the penetration depth.

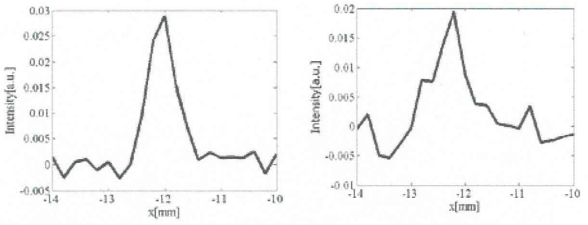

Fig.3 Lateral profile of photo-acoustic image of phantom with μ_a of 25cm^{-1} (Left : z = 12 mm, Right : z = 20 mm)

In order to evaluate resolution of PA image, full width half maximum (FWHM) in lateral direction of PA images were measured. Lateral profile of PA image of phantoms with μ_a of 25cm^{-1} placed at depth of 12 mm and 20 mm were shown in Fig.3. As shown in Fig.3, lateral FWHM 0.57 mm was obtained at depth of 12 mm and it increased at deeper region. Since this resolution corresponded to diameter of arteriolar, this method had resolution enough to image the vessels with larger diameter than arteriolar.

4. Conclusion

In this research, penetration depth and resolution of PAI were verified. They were important factors to decide the target to image. As results, blood vessel placed at 20-24 mm was detected in an ambient medium with scattering coefficient equivalent to biological tissue. Increase of laser pulse energy enables deeper tissue imaging. Furthermore, resolution enough to image arteriolar was confirmed. As next step, we discuss the appropriate target to image in clinical application.

Reference

[1] M. Xu and L. V. Wang, "Photoacoustic imaging in biomedicine", Rev. Sci. Insrum., Vol. 77, 041101, 2006

[2] H. F. Zhang, K. Maslov, G. Stoica, and L. V. Wang, " Functional Photoacoustic Microscopy for High-resolution and Noninvasive in vivo Imaging", Nat. Biotechnol., Vol.24, No.7, pp. 848-851, 2006

[3] E. Z. Zhang, J. G. Laufer, R. B. Pedley, and P. C. Beard, "In vivo High-resolution 3D Photoacoustic imaging of Superficial Vascular Anatomy", Phys. in Med. Biology, Vol.54, pp. 1035-1046, 2009

[4] T. Ohmori, M. Ishihara, K. Tsujita, I. Bansaku, and M. Kikuchi, "Multicolor Photoacoustic Imaging by a Single Transducer with Piezoelectric Copolimer Film in a wide Frequency Range", Proc. Of SPIE, Vol.7564, 75642V", 2010

[5] H. J. van Staveren, C. J. M. Moes, J. van Marle, S. A. Prahl, and M. J. C. van Gemert, "Light Scattering in Intralipid-10% in the Wavelength of 400-1100 nm", App. Opt., Vol.30, No.31, pp.4507-4514, 1991

[6] W. F. Cheong, S. A. Prahl, and A. J. Welch, "A Review of Optical Properties of Biological Tissues", IEEE Journal of Quantum Electronics, Vol.26, No.12, pp.2166-2185, 1990

[7] T.Hirasawa, M. Ishihara, M.Kitagaki, I. Bansaku, M. Fujita, and M. Kikuchi, "Analysis and Verification of Dominant Factor to Obtain the High Resolution Photo-acoustic Imaging", Proc. Of SPIE, 2011 (In print)

Comparison of Regularization Methods for Photoacoustic Image Reconstruction

Shinpei Okawa, Takeshi Hirasawa, Toshihiro Kushibiki, and Miya Ishihara

Department of Medical Engineering, National Defense Medical College (Japan)

Keywords: Photoacoustic imaging, Inverse problem, Regularization

Introduction

Photoacoustic (PA) imaging obtains the distribution of the light absorbers. The energy of the light emitted by nano-second laser is absorbed by the light absorbers in tissues. And the energy is converted into heat, which causes elastic wave due to the thermal expansion. The detected elastict wave, PA signal namely, is used to reconstruct the PA image. The high resolution feature and the principle exploiting the absorption of the light allow us to obtain precise microvasular images[1].

By taking account of the excitation light propagation described by photon diffusion equation (PDE), the optical properties and concentrations of the light absorbers in optically inhomogeneous medium can be estimated by the PA image reconstruction. Laufer et al has proposed a model-based inversion scheme reconstructing the chromophore concentration[2]. The image reconstructed by solving the model-based inverse problem is always aggravated by noise and insufficient forward modeling due to the ill-posed nature. There exist mismatches between the actual measurement conditions and the forward model, which cause artifacts and low spatial resolution image.

In this paper, we compared regularization methods, i.e. truncated singular value decomposition (TSVD)[3], Tikhonov regularization and l_1 sparsity regularization[4], for model-based PA image reconstruction. The PA forward model was constructed by PA wave equation and PDE. The relation between the PA signals and the light absorption coefficient of the light absorber was formulated by finite element method (FEM). The effects of the regularization methods on the reconstructed images were investigated.

Image reconstruction method

The propagation of the PA wave is described by PA wave equation[1]. According to the PA wave equation, the intensity of the PA signal is linearly related to the source intensity. Therefore, we obtain a linear equation, $\mathbf{m} = L\mathbf{x}$, where $\mathbf{m}$ is the vector consists of the PA signals detected in multiple positions, and L is the system matrix relating $\mathbf{m}$ to the vector $\mathbf{x}$ of the source intensities at positions in the discretized medium. $\mathbf{x}$ is proportional to the product of the absorption coefficients μ_a and the fluence rates.

On the other hand, the propagation of the excitation light is described by PDE involving μ_a of the medium[4]. The fluence rate is calculated by solving PDE. When we assume that the medium has the background of the absorption coefficient μ_a^{bg} and the perturbation $\Delta\mu_a$ due to the existence of the strong light absorber such as tumor with angiogenesis, we obtain $\mu_a = \mu_a^{bg} + \Delta\mu_a$. By linearizing the relation of $\mathbf{x}$ to μ_a, the equation relating $\mathbf{m}$ to $\Delta\mu_a$ is formulated as,

$$\mathbf{m} - \mathbf{m}^{bg} = LJ\,\Delta\mu_a, \tag{1}$$

where $\mathbf{m}^{bg}$ is the contribution of μ_a^{bg} to $\mathbf{m}$, and J is the differential coefficients. By solving the equation for $\Delta\mu_a$ with given μ_a^{bg} and $\mathbf{m}^{bg}$, μ_a is reconstructed as the image. We prepared the matrices by use of FEM. Eq.(1) was solved with TSVD and with the nonlinear optimization scheme with minimizing 2-norm of $\mathbf{x}$ (Tikhonov regularization) and 1-norm of $\mathbf{x}$ (l_1 sparsity regularization).

Conditions of numerical experiment

The medium was a square region with 50 mm on a side. The light source with near-infrared wavelength was placed at (x, y) = (0 mm, 25 mm), and that 16 ultrasound detectors were placed from x = -14 to 16 mm on y = 25 mm with an equal spacing of 2 mm. The background medium had uniformly distributed with the scattering coefficient of 1.0 mm^{-1} and μ_a^{bg} = 0.001 mm^{-1}. The strong light absorber with μ_a = 0.01 mm^{-1} with 2 mm on a side was placed at (x, y) = (0 mm, 14 mm).
FEM was used with 10,201 nodes and 20,000 triangular elements to simulate PA signals. Gaussian noise was added to the simulated **m**. The noise had the standard deviation of 1 % of the maximum of the detected PA signals. The reconstruction was carried out on pixel basis. Single pixel had 2 mm on a side.

Results and discussions

Figure 1 shows the reconstructed images with TSVD, Tikhonov and l_1 sparsity regularizations. The strong absorber was reconstructed in the correct position by each regularization method. The area and the value of μ_a, however, were quite different. By TSVD and Tikhonov regularization, the area of the strong absorber was larger than true one, and the maximum value of the reconstructed μ_a was about 10 to 20 % of the true value. TSVD caused undulation in the reconstructed image. Tikhonov regularization provided the smooth distribution of μ_a.
On the other hand, l_1 sparsity regularization reconstructed image with high spatial resolution. The area of the strong absorber was correctly reconstructed. The value of the reconstructed μ_a was about 90 % of the true one. When prior information suggests that the true distribution of μ_a is sparse, l_1 sparsity regularization reconstructs more reliable PA image than TSVD and Tikhonov regularization does.

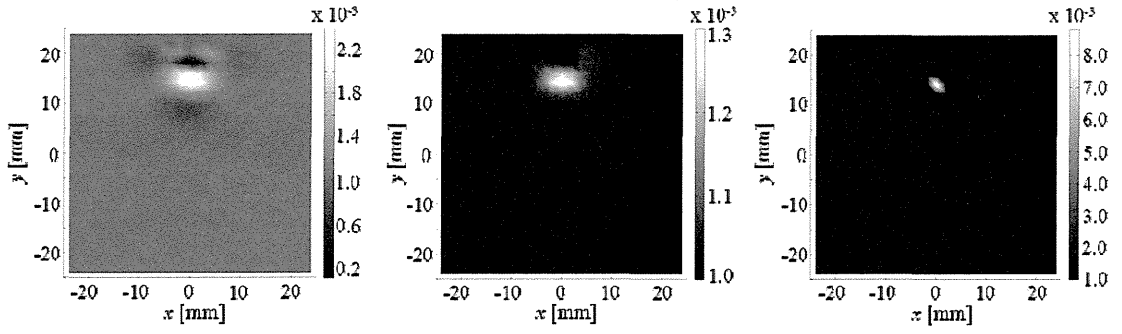

Fig. 1. Reconstructed PA images with TSVD method (left), Tikhonov regularization (center), and l_1 sparsity regularization (right).

Conclusion

The effects of the regularization methods for PA image reconstruction were compared. l_1 sparsity regularization reconstructs sparse distribution of the absorption coefficient, while TSVD and Tikhonov regularization obtain small changes in the absorption coefficient in broad area.

References

1) L. V. Wang *et al.*, Science, **335**, 1458-1462 (2012).
2) J. Laufer *et al.*, Appl. Opt., **49**, 1219-1233 (2010).
3) C. R. Vogel, Computational Methods for Inverse Problems, SIAM, (2002).
4) S. Okawa *et al.*, Biomed. Opt. Express, **2**, 3334-3348 (2012).

Development and Integration of Photoacoustic Imaging Technology

Toshihiro Kushibiki[1], Takeshi Hirasawa[1], Masanori Fujita[2], and Miya Ishihara[1]

[1]*Department of Medical Engineering, National Defense Medical College (Japan),*
[2]*Division of Environmental Medicine, National Defense Medical College Research Institute (Japan)*

Keywords: Photoacoustic, Imaging, Blood Vessel, Hemoglobin

Introduction

Optical absorption is known to associate with the biological and physiological status of living tissue. However, existing high resolution *in vivo* or *in vitro* optical imaging modalities, including confocal microscopy, two-photon microscopy and optical coherence tomography (OCT), do not sense optical absorption directly. The wideband ultrasonic waves (known as photoacoustic waves) are induced as a result of transient thermoelastic expansion of light absorbers by nano-second pulse laser irradiation to biological tissues. The photoacoustic effect is simply the generation of an acoustic wave as a result of the absorption of optical energy. While there are several mechanisms that can lead to the generation of a photoacoustic signal, biomedical photoacoustic imaging relies on the thermoelastic expansion of tissue as the photoabsorber. The light energy is absorbed by endogenous chromophores (e.g., melanin or hemoglobin) or exogenous contrast agents (e.g., dyes or nanoparticles) and converted to heat. The heat causes the tissue to undergo rapid thermoelastic expansion. The tissue then generates wideband pressure waves that originate from photoabsorbers. These pressure waves can be detected with a conventional ultrasound transducer. The photoacoustic image is created by resolving the origins of the ultrasonic waves from their arrival times. Because ultrasonic scattering is two to three orders of magnitude weaker than optical scattering in biological tissues, ultrasonic imaging can provide better spatial resolution than pure optical imaging. For the same reason, photoacoustic sources can be localized with high spatial resolution by the use of a high-frequency focused ultrasonic transducer.

In our group, we have developed the photoacoustic imaging systems for both *in vivo* and *in vitro* usage. For photoacoustic measurements, we have demonstrated that photoacoustic measurement enables viscoelastic characterization of biological tissue for diagnosis of osteoarthritis[1)]. We and our collaborators are proceeding this clinical trial and the biomechanical properties of tissue-engineered cartilage of patients are evaluated. For photoacoustic imaging (PAI), we reported the vascular imaging of mice femoral tissue by quantifying concentrations of oxy and deoxy hemoglobin. In National Defense Medical College Hospital, the clinical trials of photoacoustic imaging of vasculature are currently proceeding in the Departments of Neurosurgery and Urology in order to study on the usefulness of the photoacoustic imaging comparison to other imaging modalities such as ultrasound imaging. Furthermore, we are establishing the photoacoustic microscopy (PAM) that can generate high resolution and three-dimensional images of cells non-invasively.

In this presentation, we will introduce the principle and the advantages of photoacoustic imaging techniques compared with those of existing imaging technics, such as fluorescent imaging and OCT for *in vivo* and confocal microscopies for *in vitro*. Furthermore, we will introduce our development of photoacoustic imaging systems including both PAI and PAM.

Methods

The schematic of an experimental setup for photoacoustic imaging system is shown in Fig 1. We developed both the PAI and PAM systems to match the various imaging purpose and its target. For the comparison of the PAI and PAM, we listed the system components, imaging mode, and their resolution and penetration depth in Table 1. The PAI has an advantage to acquire the image in real-time and consequently suppress the artifact induced by body motion. A tunable Ti:sapphire laser pumped by a second-harmonic generation of Nd:YAG laser (LT2211, Lotis Tii) was used in

this study. The wavelength of this laser light was 750 nm, the range of the hemoglobin absorption, and the pulse duration was 15 ns. The collimated laser beam was coupled to an optical fiber and directed to the sample. We chose a transducer of which resonance frequency, element number, and pitch size were 10 MHz, 32 elements, and 0.31 mm, respectively. For animal model demonstration, the vascular photoacoustic imaging studies were performed on a mouse femoral tissue employing the PAI system. The transducer surface was immersed in water for ultrasound coupling. The photoacoustic data were obtained from the linear array type ultrasonic transducers during the irradiation of the laser to the sample. Through time-resolved ultrasonic detection, a 1 dimensional (1D) depth-resolved image was obtained. A tomographic image was obtained by electrically switching the active element of linear array transducers. The conventional ultrasound images were also obtained by using the high performance ultrasound inspection system (Olympus NDT).

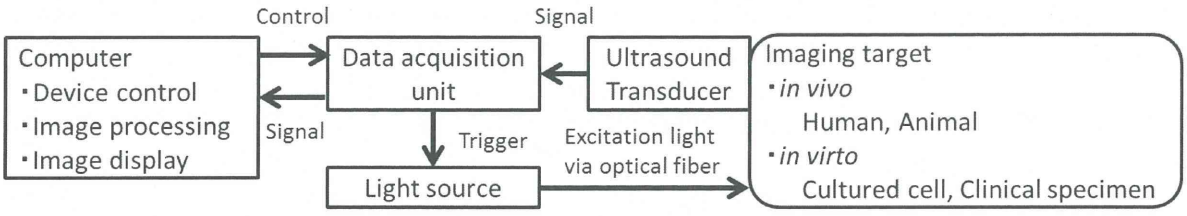

Fig. 1. The schematic of an experimental setup for photoacoustic imaging.

Table 1. The system components of PAI and PAM.

System	Light source	Ultrasonic transducer	Scanning and image reconstruction	Imaging mode	Resolution and penetration depth
PAI	Tunable, Ti:sapphire laser with high pulse energy (695–900 nm, 10 Hz, 20 mJ/pulse)	Multi-channel phased array transducer (2–10 MHz, 16–32 elements, 0.3–0.5 mm pitch)	Electrically switching of active element of the phased array transducer Reconstruction processing with back projection method	Reflection mode	Better than 1000 μm resolution and 5–10 mm penetration depth
PAM	Tunable, high repetition rate, ns-OPO (400–2600 nm, 1 kHz, ~500 μJ/pulse)	Focused single element transducer (20–50 MHz, f = 5–20 mm, Element diameter 6 mm)	Mechanical scanning of a focused transducer Directly aligning the signals acquired at each scanning position	Transmission mode	Up to 100 μm resolution and 2–3 mm penetration depth

Results

An *in vivo* photoacoustic image of the subcutaneous vasculature of the mouse femoral tissue was acquired (Fig. 2). After imaging, the blood vessels were exposed to confirm the location imaged. The image of blood vessels located on 17 mm from the surface of transducers was successfully obtained. Furthermore, we confirmed to enable the calculation of the oxygen saturation level from the obtained photoacoustic image. Thus, our technique of photoacoustic imaging can apply to the clinical diagnosis of the oxygen saturation in deep tissue.

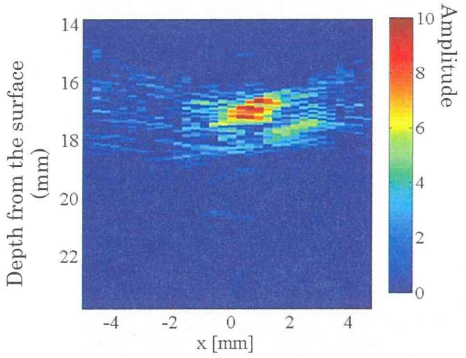

Fig. 2. *In vivo* imaging of the total hemoglobin concentration in subcutaneous vasculature of the mouse femoral tissue at 750 nm.

Acknowledgment

This research was partially supported by Health and Labour Science Research Grant for Research on Medical Device Development, and JST Collaborative Research Based on Industrial Demand (In vivo Molecular Imaging: Towards Biophotonics Innovations in Medicine).

Reference

1) M. Ishihara *et al.*, Lasers Surg. Med. **38**, 249–255 (2006).

ISSN 0385-1796

BOEI IKA DAIGAKKO ZASSHI

防衛医科大学校雑誌

Journal of the National Defense Medical College

Vol. 37 No.4 December 2012

防 医 大 誌 J. Natl. Def. Med. Coll.
37(4):243-329, 2012.

総　説

低出力レーザーにより引き起こされる生体作用

櫛引俊宏，平沢　壮，大川晋平，石原美弥

防医大誌（2012）37（4）：267－279

要旨：低出力のレーザーを用いた治療である Low Level Laser Therapy（LLLT）とは，細胞内外に存在する光受容体にレーザーのエネルギーを受容させ，引き続いて起こる生理変化を利用したものである。LLLT が提唱されて40年間で創傷治癒促進，疼痛や炎症の緩和といった有効な生物学的作用が報告されており，近年では幅広い治療分野において応用が試みられている。本論文では，LLLT に用いられている種々の光源やレーザー照射パラメーターを列挙し，これまでの著者らの報告を含めて，細胞レベルでの LLLT のメカニズムについて論じる。

索引用語：　Low Level Laser Therapy（LLLT）　／　細胞内光受容体　／　細胞機能制御

諸　言

低出力のレーザーを用いた治療である Low Level Laser Therapy（LLLT）とは，およそ数百 mW 以下の照射パワーで生体にレーザーを照射し，その生理活性変化を期待したものである。全く同じ治療方法である Low Intensity Laser Therapy（LILT）や Low Energy Laser Therapy（LELT）など多くの呼称があるが，Low Level Laser Therapy: LLLT を用いている研究者や医療従事者が多い。LLLT に用いるレーザー（LASER）は“Light Amplification by Stimulated Emission of Radiation”の頭文字をとったものであり，ランプなどから発せられる光と異なり，指向性（まっすぐ進む），単色性（波長および周波数が固定）および干渉性（位相が時間的にそろっている）に優れている。レーザーではない LED（Light Emitting Diode）やランプの光源を医療に用いる光治療である Low Level *Light* Therapy（同じく LLLT）と混同して議論されることが散見されるが，ここではレーザーを用いた LLLT について述べる。1967年，Mester らは生体組織へのレーザー照射による発がん要因の有無をテストするため，低エネルギーのレーザー（波長694nm のルビーレーザー）を剃毛したマウス背部へ照射した。その結果，発がんという結果は認められなかったが，レーザー照射部位の体毛成長速度が非照射部位に比べて促進されていることを発見した[1]。この現象は生体に対する初めてのレーザー作用の確認といわれ，LLLT の始まりであるとされている。そもそも，光を用いた治療は古くから行われており，紫外線療法も100年以上前より行われていたが[2]，光のなかでも単色性および干渉性に優れるレーザーによる生物作用は初めての報告であった。Mester らは引き続いて1971年に，レーザーを用いた LLLT の創傷治癒促進効果に関する報告を行っている[3]。それ以降，LLLT に関する報告は多岐にわたり，臨床例をはじめとして，前述の創傷治癒促進効果，コラーゲン合成促進だけではなく，細胞増殖効果，炎症抑制，疼痛緩和，骨折治癒促進や局所の血流改善など広範な生物学的効果が報告されている。一方で，Mester らの報告から35年余りを経た2003年の Journal of Clinical Laser Medicine and Surgery に，LLLT 分野では著名な Lanzafame が，“Why doesn't everyone use it?”という簡明

防衛医科大学校医用工学講座
Department of Medical Engineering, National Defense Medical College, 3-2 Namiki, Tokorozawa, Saitama 359-8513, Japan

平成24年３月15日受付
平成24年８月24日受理